

First order dynamical phase transitions

Elena Canovi,¹ Philipp Werner,² and Martin Eckstein¹

¹*Max Planck Research Department for Structural Dynamics,
University of Hamburg-CFEL, Hamburg, Germany*

²*Department of Physics, University of Fribourg, 1700 Fribourg, Switzerland*
(Dated: January 9, 2015)

Recently, dynamical phase transitions have been identified based on the non-analytic behavior of the Loschmidt echo in the thermodynamic limit [Heyl et al., Phys. Rev. Lett. **110**, 135704 (2013)]. By introducing conditional probability amplitudes, we show how dynamical phase transitions can be further classified, both mathematically, and potentially in experiment. This leads to the definition of first-order dynamical phase transitions. Furthermore, we develop a generalized Keldysh formalism which allows to use nonequilibrium dynamical mean-field theory to study the Loschmidt echo and dynamical phase transitions in high-dimensional, non-integrable models. We find dynamical phase transitions of first order in the Falicov-Kimball model and in the Hubbard model.

PACS numbers: 71.10.Fd, 64.70.Tg, 05.30.Rt

The last two decades have witnessed an extraordinary boost in the investigation of strongly correlated systems out of equilibrium, both experimentally and theoretically. This renewed interest is the consequence of the impressive experimental advances achieved in the manipulation of cold atoms in optical lattices [1–4], and in ultrafast time-resolved spectroscopy in solids [5–7]. Using systems of cold atoms, which are very well isolated from the environment and easily tunable, one can now address fundamental and long-standing problems in statistical physics. In particular, many intriguing phenomena have recently been uncovered in relation to the relaxation of excited many-body states towards thermal equilibrium [8]. Thermalization can be hampered due to (near) integrability [9] and delayed by pre-thermalization [10–12], and the different relaxation regimes can be separated by a narrow crossover as a function of some parameter [13, 14]. Near symmetry-breaking phase transitions, the dynamics can be altered entirely by the presence of non-thermal critical points [15–17]. An unsolved question in this context is whether some of these dynamical crossover phenomena reflect an underlying “sharp” transition, involving a mathematical non-analyticity of some nature.

In the transverse-field Ising model, Heyl et al. [18] found a non-analytic time-dependence of the Loschmidt echo, i.e., the probability to return to the initial state within a non-trivial time-evolution. Although the latter is not directly related to the time-dependence of thermodynamic observables, this observation suggests an intriguing new starting point for analyzing and classifying the dynamical behavior of many-particle systems. To be more precise, we consider a quantum quench, i.e. a sudden change of the Hamiltonian from some $H(t < 0) = H_0$ to $H(t \geq 0) = H$, which triggers a nontrivial out-of-equilibrium evolution. Heyl et al. [18] defined a dynamical phase transition (DPT) as a non-analytic behavior of the return probability amplitude [19]

$$A(t) = \langle \psi_0 | e^{-iHt} | \psi_0 \rangle \quad (1)$$

as a function of time, where $|\psi_0\rangle$ is the ground state of H_0 . The return probability, defined by $L(t) \equiv |A(t)|^2$, is the Loschmidt echo. In analogy to the equilibrium partition function, which has a large deviation form $Z = \text{Tr} e^{-\beta H} \sim e^{-\beta N f(\beta)}$ in the thermodynamic limit $N \rightarrow \infty$ with a free energy density $f(\beta)$, $A(t)$ has a large deviation limit of the form $A(t) \sim e^{-Na(it)}$, and non-analytic behavior as a function of time can occur in the thermodynamic limit [20].

Since the seminal work [18], further progress has been achieved in the understanding of DPTs [21–29], but important questions remain open. Firstly, the Loschmidt echo is the probability of performing no work in a double quench experiment $H_0 \rightarrow H \rightarrow H_0$ [18], but it is not in any obvious, simple way related to the time-evolution of physical observables, which also hampers a further characterization and classification of DPT’s. Furthermore, DPTs may be hard to access in non-integrable systems which do not allow for an exact solution: the computation of an overlap amplitude is most direct with wavefunction based numerical techniques, which are however almost exclusively used for finite or one-dimensional systems. Examples thereof are exact diagonalization, which is restricted to small systems, or infinite DMRG [26]. In this Letter we present two concepts to address these questions: first we introduce conditional amplitudes and generalized expectation values, which allow for a further classification of DPTs and also for the definition of first order transitions. Second, we explain how the amplitude (1) can be computed with diagrammatic many-body techniques and nonequilibrium dynamical mean-field theory [30], which makes it accessible for a large class of high-dimensional, interacting models directly in the thermodynamic limit.

First-order dynamical phase transitions — As Eq. (1) gives the probability amplitude for the return to the initial state $|\psi_0\rangle$, a natural way to further classify a DPT is to more closely characterize the “path” along which this

return happens. As we will see, a first-order DPT occurs when these paths for infinitesimally different propagation times t can be distinguished by a nonvanishing change in a *macroscopic* measurement. To illustrate this idea, let $\hat{X} \equiv N\hat{x}$ be any observable which is extensive in the system size N . Then we can define a *conditional return amplitude*

$$\tilde{A}(t, x)\Delta x \equiv \langle \psi_0 | e^{-iH(t-t_1)} \mathcal{P}_x^{\Delta x} e^{-iHt_1} | \psi_0 \rangle, \quad (2)$$

where $\mathcal{P}_x^{\Delta x}$ can be any operator that selects eigenstates of \hat{x} with eigenvalues in a small interval of size Δx around x , e.g., $\mathcal{P}_x^{\Delta x} \propto \sum_i e^{-[i|\hat{x}|i-x]^2/2\Delta x^2} |i\rangle\langle i|$. (Note that this choice implies that \mathcal{P} , and hence $\tilde{A}(t, x)$, is a smooth function of x for finite systems). In a many-body path integral formulation [31], Eq. (1) can be written as the sum over all paths in some configuration space (Grassmann variables for fermions, complex fields for bosons), with a boundary condition provided by the state $|\psi_0\rangle$, while $\tilde{A}(t, x)$ sums the sub-class of paths fixed by the constraint $\hat{x} = x$ at the intermediate time $t = t_1$. By construction, we have $A(t) = \int dx \tilde{A}(t, x)$. Assuming again a large deviation form $\tilde{A}(t, x) = e^{-N\tilde{a}(it, x)}$ for $N \rightarrow \infty$, the integral will be dominated by its saddle-point values, i.e., $a(it) = \tilde{a}(it, x_*(t))$, where the complex number $x_*(t)$ is determined by $d\tilde{a}/dx|_{x=x_*} = 0$. In the presence of several saddle-points the dominant one can change as a function of the parameter t , which defines a first order dynamical transition, in analogy to first order transitions in equilibrium. Because such a first order transition is a change of the propagator (1), its detection should not depend on the particular choice of \hat{x} or t_1 , but should be reflected by an abrupt change of the *generalized expectation value* of a generic observable \hat{Y} ,

$$\langle \hat{Y}(t_1) \rangle_A = A(t)^{-1} \langle \psi_0 | e^{-iH(t-t_1)} \hat{Y} e^{-iHt_1} | \psi_0 \rangle. \quad (3)$$

which is obtained from $A(t)$ by an infinitesimal variation $\langle \hat{Y}(t_1) \rangle_A = i \frac{\delta \ln A_\eta(t)}{\delta \eta(t_1)} |_{\eta=0}$, of a field $\eta(t')$ coupling to \hat{Y} , with $A_\eta(t) = \langle \psi_0 | T_t \exp[-i \int_0^t dt' (H + \eta(t')\hat{Y})] | \psi_0 \rangle$. One of the main results of this work is that both the expectation values Eq. (3) and the rate $a(it)$ can be easily computed within the DMFT formalism, as we show later. It follows from the discussion above that the expectation value of \hat{x} yields the complex saddle point $x_*(t)$, which abruptly changes as a function of t .

Before discussing first-order DPTs' in specific models, it is important to note how generalized expectation values are related to real measurements, in spite of the fact that the quantity $\langle \hat{Y} \rangle_A$ itself is in general complex and only real probabilities like the Loschmidt echo can be considered measurable. To make the connection, we consider the Loschmidt echo, $L_{\delta t}(t) \equiv |\langle \psi_0 | e^{-iH(t-t_1)} e^{-ig\hat{Y}\delta t} e^{-iHt_1} | \psi_0 \rangle|^2$ of an experiment with an extended quench protocol involving a quench $H_0 \rightarrow H$ at time zero, a short intermediate propagation from t_1 to

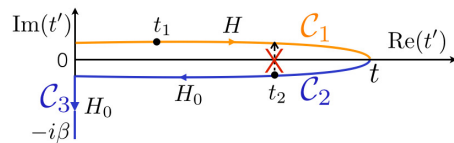


FIG. 1. (color online) Generalized contour-dependent Hamiltonian on the Keldysh contour \mathcal{C} . The upper, lower and imaginary branches of the contour are denoted by \mathcal{C}_1 , \mathcal{C}_2 and \mathcal{C}_3 respectively. The arrows indicate the contour ordering, in this case t_1 comes earlier than t_2 , i.e. $t_1 < t_2$. For a Green function $G(t_1, t_2)$, if t_1 lies on \mathcal{C}_1 and t_2 lies on \mathcal{C}_2 , the latter cannot be shifted to the upper contour.

$t_1 + \delta t$ with a Hamiltonian $g\hat{Y}$, and a final propagation with H [32]. Taking the limit of small δt yields:

$$L_{\delta t}(t) / L(t) = 1 + 2g\delta t \text{Im}\langle \hat{Y} \rangle_A + \mathcal{O}(g^2\delta t^2). \quad (4)$$

In essence, the intermediate propagation adds a phase kick to the propagator, thus measuring the imaginary part of $\langle \hat{Y} \rangle_A$.

Dynamical mean-field theory — We now proceed to explain how the Loschmidt amplitude rate $a(it)$ and the expectation values (3) can be computed for high-dimensional fermionic lattice systems. In the study of quantum systems out of equilibrium, one of the most powerful techniques is dynamical mean-field theory (DMFT) [30, 33], which captures local correlations in high-dimensional systems, by mapping a lattice model onto an effective impurity model. This mapping is exact in the limit of infinite dimensions [34]. Here we use it to study the generic correlated lattice model

$$H(t) = H_0 + U(t) \sum_i n_{i\uparrow} n_{i\downarrow} \quad (5)$$

with $H_0 = -\sum_{\langle i,j \rangle \sigma} t_\sigma V_{ij} c_{i\sigma}^\dagger c_{j\sigma} + \mu \sum_{i\sigma} n_{i\sigma}$, which describes fermions with two (spin) flavors on a lattice: V_{ij} are lattice-dependent hoppings, t_σ is a spin-dependent prefactor of the hopping term, and $n_{i\sigma} = c_{i\sigma}^\dagger c_{i\sigma}$. The time-dependent local repulsion energy $U(t)$ is the parameter driving the sudden quench from H_0 to H : $U(t \leq 0) = 0$ and $U(t > 0) = U$. The Hamiltonian (5) describes the Falicov-Kimball model when one spin flavor is localized ($t_\downarrow = 0$), and the Hubbard model when $t_\uparrow = t_\downarrow = 1$ (see below).

Nonequilibrium DMFT is based on the many-body Keldysh formalism, which is formulated in terms of Green's functions and thus does not directly give access to wave-function overlaps like in Eq. (1). In order to use a Green's function formalism to compute the overlap, we first introduce in Eq. (1) an identity $e^{-iH_0 t} e^{iH_0 t}$ and a fictitious temperature $1/\beta$, which is then sent to zero,

$$A(t) = \lim_{\beta \rightarrow \infty} e^{E_0(\beta-it)} \text{Tr} \left(e^{-\beta H_0} e^{iH_0 t} e^{-iHt} \right). \quad (6)$$

Formally, we can view the terms under the trace as the time-ordering of a *generalized contour-dependent Hamiltonian* (GCH) defined on the Keldysh contour $\mathcal{C} = \mathcal{C}_1 \cup \mathcal{C}_2 \cup \mathcal{C}_3$,

$$\mathcal{Z}_{\mathcal{C}} \equiv \text{Tr} \left(\mathcal{T}_{\mathcal{C}} e^{-i \int_{\mathcal{C}} dt' H_{\mathcal{C}}(t')} \right), \quad (7)$$

where the Hamiltonians $H_{\mathcal{C}}(t)$ on the upper (\mathcal{C}_1) and lower (\mathcal{C}_2) real branches are different, $H_{\mathcal{C}}(t) = H$ for $t \in \mathcal{C}_1$ and $H_{\mathcal{C}}(t) = H_0$ for $t \in \mathcal{C}_{2,3}$ (see Fig. 1). We can define contour-ordered expectation values $\langle \mathcal{O} \rangle_{H_{\mathcal{C}}} = \text{Tr}[\mathcal{T}_{\mathcal{C}} e^{-i \int_{\mathcal{C}} dt' H_{\mathcal{C}}(t')} \mathcal{O}(t_1)] / \mathcal{Z}_{\mathcal{C}}$, which coincide with the generalized expectation values (3) in the limit $\beta \rightarrow \infty$.

At this point we note that the Keldysh formalism remains applicable when the Hamiltonian is an explicit function of the contour time. In particular, diagrammatic rules for contour-ordered Green's functions $G_{ij}(t_1, t_2) = -i \langle \mathcal{T}_{\mathcal{C}} c_i(t_1) c_j^\dagger(t_2) \rangle_{H_{\mathcal{C}}}$ remain unchanged, and one can define a self-energy and a Dyson equation formally identical to those for the standard contour Hamiltonian. With this, any argument leading to the DMFT formalism, based on either power counting or the cavity formalism [33] can be rewritten one-to-one for a generic contour-dependence of $H_{\mathcal{C}}$. We use DMFT with GCHs to study the Falicov-Kimball and the Hubbard model, in the former using closed equations of motion, in the latter employing a Quantum Monte Carlo algorithm [35]. Details on the DMFT solution and its implementation are given in the Supplemental Material.

Within the Green's function formalism, the overlap amplitude (6) is obtained from a coupling constant formalism. Taking the derivative of the free energy $a_U(it) = \lim_{N \rightarrow \infty} -(1/N) \ln A_U(t)$ involves the generalized expectation value of the double occupancy $d = \frac{1}{N} \sum_i n_{i\uparrow} n_{i\downarrow}$,

$$\frac{\partial a_U(it)}{\partial U} = -i \lim_{\beta \rightarrow \infty} \int_0^t dt' \langle d(t') \rangle_{H_{\mathcal{C}}(U)}, \quad (8)$$

where the dependence of A [Eq. (6)] and $H_{\mathcal{C}}$ on the parameter U in H is made explicit. For convenience, we also define the integrated double occupancy $\Delta(U, t) \equiv (1/t) \int_0^t dt' \langle d(t') \rangle_{H_{\mathcal{C}}(U)}$. The free energy is then just the integral of (8), i.e. $a(it) = \lim_{\beta \rightarrow \infty} it \int_0^U dU' \Delta(U', t)$.

Results — As a first application of the above results, we focus on the Falicov-Kimball model (FKM). It describes two species of fermions: the itinerant ones, which can hop between neighboring sites, and the immobile ones, which act as an annealed disorder potential for the other species. The Hamiltonian is given by Eq. (5) with hopping $t_\sigma = 0$ for one species. The FKM can be solved exactly within DMFT [36]. It displays a rich phase diagram [37], including a paramagnetic metal-insulator transition at half-filling ($\langle n_\uparrow \rangle = \langle n_\downarrow \rangle = \frac{1}{2}$) which is located at $U_c = 2$ (independent of temperature) for the Bethe lattice. The possibility of an exact solution makes the FKM an important benchmark also for nonequilibrium DMFT

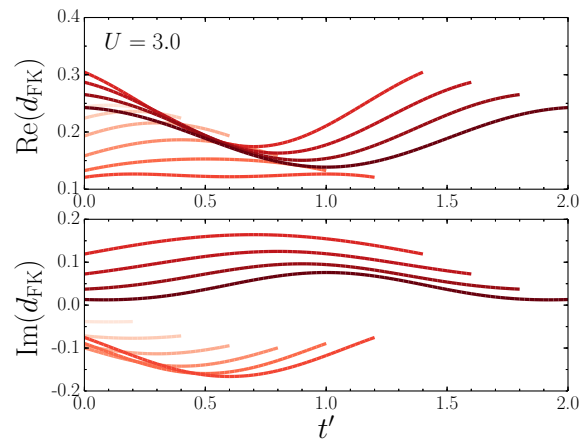


FIG. 2. (Color online) Time-dependent generalized expectation value of the double occupancy $d_{FK}(t') \equiv \langle d(t') \rangle_{H_{\mathcal{C}}}$ in the FKM for $U = 3.0$ and increasing values of t from $t = 0.2$ to $t = 2.0$ (t is evident from the length of the contour, $0 \leq t' \leq t$). Upper panel: real part, lower panel: imaginary part. Data obtained with $\beta = 50$, real-time discretization step $dt = 0.02$ and a mesh of $N_\tau = 200$ points on the imaginary axis (see the Supplemental Material for technical details).

[38–42], in spite of the peculiarity that thermalization is excluded because of the missing interaction between the itinerant fermions [40]. The DMFT equations for a GCH, which are analogous to the standard nonequilibrium DMFT solution [38], are given in the Supplemental Material.

We will now show that the FKM undergoes a DPT. As can be seen in Fig. 2, our DMFT results indicate that the time-dependent generalized expectation value of the double occupation abruptly changes its shape with increasing t (see for example the curves at $t = 1.2$ and 1.4). In Fig. 3 we plot the integrated double occupancy $\Delta(U, t)$ as a function of U for given t . We indeed find a non-analytic curve, which displays a sequence of jumps in whose vicinity two coexisting DMFT solutions for d_{FKM} are found. The coexistence of solutions evidences a *first-order* dynamical transition. We map out the coexistence region (shaded area in the Figure) by increasing (decreasing) U in small steps, using the solution at a given U as a starting input for the DMFT iteration at the next value of the interaction. In the lower panel of Fig. 3 blue squares give the bounds of the coexistence region obtained in this way, indicating a transition for quenches to all values $U > U_c$.

We have also applied our generalized Keldysh formalism to the Hubbard model, which describes correlated fermions with spin- $\frac{1}{2}$ on a lattice. A numerically exact solution of the nonequilibrium DMFT equations can be obtained with a continuous-time Monte Carlo impurity solver. The weak-coupling approach [35, 43] allows to simulate reasonably long time intervals, especially in the present set-up, where the time-evolution starts from a

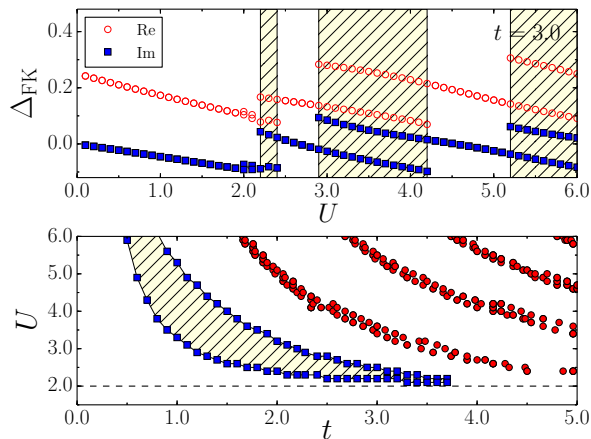


FIG. 3. (Color online) Dynamical phase diagram of the FKM. Top: real and imaginary part of the integrated double occupation Δ_{FKM} obtained by increasing (decreasing) U in steps of $\Delta U = 0.1$ from $U = 0.1$ ($U = 6.0$), and using the solution at U as a seed for the iterative solution of DMFT at $U + \Delta U$ ($U - \Delta U$). Bottom: Blue squares show the coexistence region around the first transition branch, obtained at each t as described in the upper panel. For the other transition branches, we provide only lower-bound estimates for the coexistence region: In the region between red dots at the same t , two coexisting solutions are found by different choices in the update of the Green function at each DMFT iteration (see Supplemental Material).

non-interacting equilibrium state, and where interaction vertices only have to be sampled on the forward branch \mathcal{C}_1 . However, since the Green functions for GCHs lack causal symmetries (see Supplemental Material), we cannot use the improved estimator introduced in Ref. 35, which makes the calculations time-consuming.

Our results demonstrate that the Hubbard model also exhibits a first-order DPT. In Fig. 4 (a) we show that the integrated double occupation after a quench in the strong coupling regime ($U = 10$) has a jump at $t \sim 0.85$. As in the case of the FKM, the first-order nature of the transition is signaled by a coexistence of solutions, as shown in Fig. 4 (b). In contrast to the FKM, which is peculiar in the sense that even in equilibrium the metal-insulator transition prevails to all temperatures, the Hubbard model is a non-integrable model which does show thermalization after a quench [13].

Conclusions – This paper provides two main insights related to the study of DPTs. From a theoretical point of view, we have shown that dynamical phase transitions can be more deeply characterized by means of conditional probability amplitudes and generalized expectation values, which are experimentally accessible with suitable quench protocols. From a methodological point of view, our main result is that the Loschmidt echo can be obtained in the context of DMFT by considering a general contour-dependent Hamiltonian on the Keldysh contour.

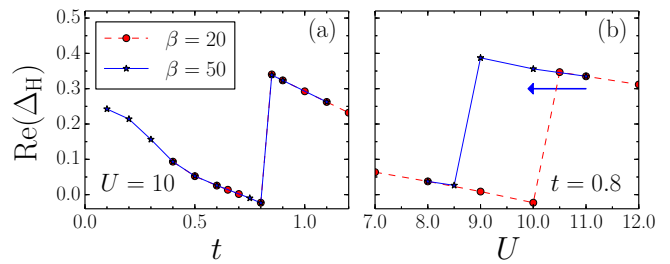


FIG. 4. (Color online) DPT in the Hubbard model. Panel (a): Real part of the integrated double occupation for a quench to $U = 10$ at different t . To confirm the convergence of the results with the fictitious temperature, we show data for $\beta = 20$ (red circles) and $\beta = 50$ (blue stars). Panel (b): coexisting solutions for $\Delta_{\text{H}}(U)$ at $t = 0.8$ at different values of U . Red circles and blue stars are obtained using as an initial guess for the hybridization function in DMFT the noninteracting Green function on the Bethe lattice and the converged solution at $U = 11$ respectively.

We find first order DPTs both for the Falicov-Kimball and the Hubbard model. This raises the hope to actually observe DPTs in experiments with cold atoms, although issues like finite size effects and the influence of the trap remain to be investigated. In future work we plan to map out the precise phase diagram, including the location of the discontinuities, which requires extensive numerical calculations to perform the additional coupling constant integral. The presence of first-order DPTs in the FKM and the Hubbard model can shed new light on the previous works on DPTs. For example, there are indications that the non-analyticity of the Loschmidt rate found in the Ising model [18] and its nonintegrable variants [26, 29] are of first-order: the analytical expressions in Ref. [18] show that the generalized expectation value of the transverse magnetization M , which is a derivative of the Loschmidt rate with respect to the magnetic field, shows a jump at the critical times. (More recent work on 2-band systems indicates transitions of different order [44]). An intriguing problem would thus be to compute also conditional amplitudes (2) as a function of time and M in this exactly solvable model, and thus to characterize the analytical structure of the transition in this model.

We thank K. Balzer, R. Fazio, M. Heyl, S. Kehrein, M. Kollar, J. Mentink, D. Rossini, and S. Sayyad for useful discussions. The QMC calculations used a code based on ALPS [45]. PW is supported by FP7/ERC starting grant No. 278023.

Supplemental Material

Green's functions for a contour-dependent Hamiltonian

In the main text we have introduced the Keldysh formalism for a generalized contour-dependent Hamiltonian (GCH) which is different on the two real-time branches of the Keldysh contour \mathcal{C} (H_0 on the upper and H on the lower branch, respectively.) As already mentioned, the diagrammatic rules remain unchanged if the Hamiltonian depends explicitly on the contour branch, and one can define Green's functions G , self-energies Σ , and a Dyson equation formally identical to the standard nonequilibrium case,

$$G = G_0 + G_0 * \Sigma * G = G_0 + G * \Sigma * G_0. \quad (9)$$

(G_0 is the noninteracting Green's function, and the $*$ -symbol denotes the convolution along \mathcal{C} .) In spite of the formal analogy, there are important differences concerning the symmetry of the Green's functions, which have to be taken into account in numerical manipulations. In this section we explain these differences and give details of the numerical implementation of contour convolutions and the inversion of the Dyson equation.

Contour-ordered Green's functions

Contour-ordered expectation values for a GCH are defined in analogy to the standard nonequilibrium formalism (see Ref. [30] for an introduction to the Keldysh formalism and for the notation used in in this text),

$$\langle \dots \rangle_{H_C} \equiv \frac{\text{tr}[\mathcal{T}_C e^{-i \int_C dt' H(t')} \dots]}{\text{tr}[\mathcal{T}_C e^{-i \int_C dt' H(t')}]} \quad (10)$$

Here the contour-ordering is defined as usual, by

$$\mathcal{T}_C \mathcal{A}(t) \mathcal{B}(t') \equiv \theta_C(t, t') \mathcal{A}(t) \mathcal{B}(t') \pm \theta_C(t', t) \mathcal{B}(t') \mathcal{A}(t), \quad (11)$$

where the upper (lower sign) is for bosonic (fermionic) operators, and

$$\theta_C(t, t') = \begin{cases} 1 & t \succ t' \\ 0 & \text{else,} \end{cases} \quad (12)$$

with $t \succ t'$ ($t \prec t'$) meaning that t comes later (earlier) than t' in the sense of the contour. Green's functions are defined as

$$G(t, t') = -i \langle \mathcal{T}_C c(t) c^\dagger(t') \rangle_{H_C}. \quad (13)$$

As in the standard nonequilibrium case, cyclic invariance of the trace implies a boundary condition of the Green's functions,

$$G(0^+, t) = \pm G(-i\beta, t) \quad (14)$$

$$G(t, 0^+) = \pm G(t, -i\beta), \quad (15)$$

where $0^+ \in \mathcal{C}_1$ and $-i\beta \in \mathcal{C}_3$.

Because each of its times arguments t and t' can lie on three different branches, the Green's function (13) has 9 components $G(t, t') \equiv G_{ij}(t, t')$ ($t \in \mathcal{C}_i$, $t' \in \mathcal{C}_j$, $i, j = 1, 2, 3$):

$$\hat{G} = \begin{pmatrix} G_{11} & G_{12} & G_{13} \\ G_{21} & G_{22} & G_{23} \\ G_{31} & G_{32} & G_{33} \end{pmatrix}. \quad (16)$$

In the standard nonequilibrium case, these 9 components are not independent from each other: one can always shift the operator with the largest real-time argument from \mathcal{C}_1 to \mathcal{C}_2 and vice-versa, because the backward and forward time evolution operator for larger times cancel. Various (time-propagating) approaches found in the literature [46–50] exploit these symmetries, to transform contour-equations into causal time-propagation equations (Kadanoff-Baym equations). However, these symmetries are apparently lost when the Hamiltonian on \mathcal{C}_1 and \mathcal{C}_2 is different, so that $G_{11}(t, t') \neq G_{12}(t, t')$ even for $t \leq t'$, $G_{13}(t, \tau') \neq G_{23}(t, \tau')$, and so on. To manipulate Green's function for a GCH we thus do not use Kadanoff-Baym equations, but stick to an approach based on the explicit discretization of \mathcal{C} (similar to what has been used in Ref. [39] for the standard nonequilibrium case).

Discretization of the contour

Each of the real-time branches of \mathcal{C} is divided in N_t intervals, equally spaced with a time step Δt . The results presented in this work are obtained with $\Delta t = 0.02$. Introducing the convention that time on the upper (lower) real contour is indicated with t^+ (t^-), the discretized points are $\{t_0^+ = 0, t_1^+ = \Delta t, \dots, t_{N_t-1}^+ = (N_t - 1)\Delta t, t_{N_t}^+ = N_t \Delta t = t_{\max}\}$ and $\{t_{N_t}^- = N_t \Delta t = t_{\max}, t_{N_t-1}^- = (N_t - 1)\Delta t, \dots, t_1^- = \Delta t, t_0^- = 0\}$ on \mathcal{C}_1 and \mathcal{C}_2 respectively. The point $t = t_{\max}$ is thus present twice on the discretized contour, so that there are totally $2N_t + 2$ points on the real branches.

Since we have to take the limit of large β to study dynamical transitions, particular care has to be taken in the discretization of the imaginary branch. We will take advantage of the fact that the Green's functions on the imaginary branch vary rapidly only near $\tau \gtrsim 0$ and $\tau \lesssim \beta$, while they vary slowly elsewhere, and employ a nonlinear mesh such that the regions $\tau \gtrsim 0$ and $\tau \lesssim \beta$ are more densely sampled than the rest of the interval. To this aim, we first define a mapping from a variable $x \in [0, 1]$ to the imaginary time $\tau \in [0, \beta]$ via a function $f(x)$:

$$\tau \equiv \beta f(x), \quad (17)$$

with a positive derivative $f'(x)$. The linear mesh is trivially recovered with the function $f(x) = x$. In our calculations we choose a hyperbolic-tangent mesh defined as

follows:

$$f(x) = c_1 + \frac{c_2}{2} (\tanh[\alpha(2x - 1)] + 1), \quad (18)$$

where $c_1 = -\frac{\rho}{1-2\rho}$, $c_2 = \frac{1}{1-2\rho}$ and $\rho = \frac{1}{2}(1 - \tanh(\alpha))$. With this definition $f(0) = 0$ and $f(1) = 1$. We typically take $\alpha = 4.0$ to ensure a sufficiently steep function. We then discretize the variable x , splitting the interval $[0, 1]$ into N_τ equally spaced points $x_0 = 0, x_1 = \Delta x, \dots, x_{N_\tau-1} = (N_\tau-1)\Delta x, x_{N_\tau} = N_\tau\Delta x$, with $\Delta x = 1/N_\tau$. The nonlinear mesh is now composed of the $N_\tau + 1$ points $\{\tau_n = f(x_n) = f(n\Delta x)\}$. On the discretized contour the $t^- = \tau = 0$ point is doubly defined: as $t_0^- = 0$ on \mathcal{C}_2 and as $\tau_0 = 0$ on \mathcal{C}_3 .

Summarizing, the contour is composed of $N_1 = N_t + 1$ equally spaced points on \mathcal{C}_1 , $N_2 = N_t + 1$ equally spaced points on \mathcal{C}_2 and $N_3 = N_\tau + 1$ inhomogeneously spaced points on \mathcal{C}_3 , giving a total of $N \equiv 2N_t + N_\tau + 3$ points.

Matrix form of the Green's function

With the discretization of time described above, the Green's function is represented as a $N \times N$ matrix $\bar{G}(t_n, t_m)$, with $n, m = 0, \dots, N - 1$. Since Green's functions are discontinuous at equal times, we store an additional N -component vector $\Delta G(t_n)$, which takes into account the discontinuity. In our implementation, the diagonal element $\bar{G}(t_n, t_n)$ contains the average of the lesser and greater components, while the vector contains the difference:

$$\bar{G}(t_n, t_n) \equiv \frac{1}{2}(G^{<, \text{real}}(t_n, t_n) + G^{>, \text{real}}(t_n, t_n)) \quad (19)$$

and

$$\Delta G(t_n) \equiv \frac{1}{2}(G^{<, \text{real}}(t_n, t_n) - G^{>, \text{real}}(t_n, t_n)). \quad (20)$$

The superscripts mean the following: $<, \text{real}$ ($>, \text{real}$) refers to the Green's function $G(t, t')$ with $t < t'$ ($t > t'$) in the sense of *real* time (analogously with $\tau < \tau'$ ($\tau > \tau'$) if the imaginary time is defined with $-i\tau$ with $0 \leq \tau \leq \beta$). This does *not* coincide with lesser (greater) in the sense of the contour if, for example, t and t' lie on the lower \mathcal{C}^- real branch.

We also introduce a convenient rescaling of the Green's functions on the imaginary branch which incorporates the nonlinear mesh. It consists in multiplying the Green's function by a factor $\sqrt{\beta f'}$ for each imaginary time:

$$G(t, \tau) \rightarrow \tilde{G}(t, x) \equiv \sqrt{\beta f'(x)} G(t, \tau(x)) \quad (21)$$

$$G(\tau, t) \rightarrow \tilde{G}(x, t) \equiv \sqrt{\beta f'(x)} G(\tau(x), t), \quad (22)$$

$$G(\tau, \tau') \rightarrow \tilde{G}(x, x') \equiv \sqrt{\beta f'(x)} \sqrt{\beta f'(x')} G(\tau(x), \tau(x')). \quad (23)$$

As we shall see below, the advantage of this rescaling is that the convolution has the same numerical implementation on the entire contour.

Convolutions

The fundamental operation to be implemented for Green's functions is the convolution, which is formally defined as an integral on the contour:

$$C(t, t') \equiv [A * B](t, t') \equiv \int_{\mathcal{C}} d\bar{t} A(t, \bar{t}) B(\bar{t}, t'). \quad (24)$$

From the numerical point of view, two issues must be taken into account in the computation of the convolution: the nonlinear mesh on the imaginary branch and the effect of the jump of the Green's functions A and B at $t = t'$.

Concerning the nonlinear mesh, let us consider the convolution $C(t, t')$ of two Green's functions $A(t, t')$ and $B(t, t')$ (Eq. (24)) and split it into the three contributions coming from the different branches $\mathcal{C}_1, \mathcal{C}_2$ and \mathcal{C}_3 :

$$C(t, t') = C_1(t, t') + C_2(t, t') + C_3(t, t'). \quad (25)$$

The rescaling of Eqs. (21)-(23) allows to write the convolution in terms of the (equally spaced) variable x in a straightforward way. As an example, we compute the contribution on the imaginary branch to the Matsubara component of C :

$$C_3(\tau, \tau') = \int_0^\beta d\bar{\tau} A(\tau, \bar{\tau}) B(\bar{\tau}, \tau') \quad (26)$$

Performing a change of integration variable $\bar{\tau} = \beta f(\bar{x})$ and using Eq. (23), we can rewrite Eq. (26) as

$$C_3(\tau, \tau') = \int_0^1 d\bar{x} \beta f'(\bar{x}) \frac{\tilde{A}(x, \bar{x}) \tilde{B}(\bar{x}, x')}{\sqrt{\beta f'(x)} \sqrt{\beta f'(x')} \beta f'(\bar{x})}, \quad (27)$$

which implies

$$\tilde{C}_3(x, x') = \int_0^1 d\bar{x} \tilde{A}(x, \bar{x}) \tilde{B}(\bar{x}, x'). \quad (28)$$

From Eq. (28) we see that integration on the imaginary branch can be performed on the equally-spaced variable x at the cost of a simple rescaling (Eqs. (21)-(23)) of the Green's functions.

In order to clarify how to include the contributions of the jumps of $A(t, t')$ and $B(t, t')$, we need first to specify how the integrals are discretized on the contour. We found it convenient and efficient to use the trapezoidal rule, so that we can generically write \tilde{C} as the result of a matrix multiplication:

$$\tilde{C} = \tilde{A} \tilde{W} \tilde{B}, \quad (29)$$

where \tilde{A} and \tilde{B} are defined as in Eq. (19) and \tilde{W} is a diagonal matrix $(\tilde{W})_{nm} = \delta_{nm} w_n$ containing the integration

weights. The vector \bar{w} is composed of three parts, each corresponding to a different branch:

$$\bar{w} = \begin{pmatrix} \bar{w}^{(1)} \\ \bar{w}^{(2)} \\ \bar{w}^{(3)} \end{pmatrix}, \quad (30)$$

where

$$w_0^{(1)} = w_{N_t}^{(1)} = \frac{1}{2}\Delta t, \quad w_j^{(1)} = \Delta t \text{ if } j \neq 0, N_t, \quad (31)$$

$$w_0^{(2)} = w_{N_t}^{(2)} = -\frac{1}{2}\Delta t, \quad w_j^{(2)} = -\Delta t \text{ if } j \neq 0, N_t, \quad (32)$$

$$w_0^{(3)} = w_{N_\tau}^{(3)} = -i\frac{1}{2}\Delta x, \quad w_j^{(3)} = -i\Delta x \text{ if } j \neq 0, N_\tau, \quad (33)$$

and in the third line we have used the form (28) of the integral on the imaginary branch. At this point it is important to remark that $C(t, t')$ itself has no jumps, i.e. $\Delta C(t_n) = 0$, so the only thing we have to compute is the matrix \tilde{C} . However, Eq. (29) alone is not correct, because it does not take into account the discontinuities of A and B on the diagonal. For this reason, we need to compute corrections to Eq. (29). Suppose we want to compute the diagonal element $C(t, t)$ (with $t \in \mathcal{C}_1$), and in particular the contribution of the upper real branch, i.e. $C_1(t, t) = \int_0^{t_{\max}} d\bar{t} A(t, \bar{t})B(\bar{t}, t)$ (see Eq. (25)). Using Eq. (24), the integral can be exactly rewritten as:

$$C_1(t, t) = \int_0^t d\bar{t} A^{>, \text{real}}(t, \bar{t})B^{<, \text{real}}(\bar{t}, t) + \int_t^{t_{\max}} d\bar{t} A^{<, \text{real}}(t, \bar{t})B^{>, \text{real}}(\bar{t}, t). \quad (34)$$

With the discretization described above and the integration weights Eqs. (30) and (31), the discretized form of Eq. (34) reads

$$(C_1)_{nn} = \left\{ \sum_{l=1}^{n-1} \bar{A}_{nl} \bar{B}_{ln} + \sum_{l=n+1}^{N_t-1} \bar{A}_{nl} \bar{B}_{ln} + \frac{1}{2} \bar{A}_{n0} \bar{B}_{0n} + \frac{1}{2} \bar{A}_{nN_t} \bar{B}_{N_t n} + \frac{1}{2} A_{nn}^{>, \text{real}} B_{nn}^{<, \text{real}} + \frac{1}{2} A_{nn}^{<, \text{real}} B_{nn}^{>, \text{real}} \right\} \Delta t, \quad (35)$$

where $t = n\Delta t$ and we used the short notation $\bar{A}(t_n, t_m) \equiv \bar{A}_{nm}$. The only approximation in Eq. (35) with respect to Eq. (34) is the discretization of time, which in this case gives an error $\propto \Delta t^2$. What we actually find from Eq. (29), using the representation Eq. (19)

of the diagonal elements, is different:

$$(\tilde{C}_1)_{nn} = \left\{ \sum_{l=1}^{n-1} \bar{A}_{nl} \bar{B}_{ln} + \sum_{l=n+1}^{N_t-1} \bar{A}_{nl} \bar{B}_{ln} + \frac{1}{2} \bar{A}_{n0} \bar{B}_{0n} + \frac{1}{2} \bar{A}_{nN_t} \bar{B}_{N_t n} + \frac{1}{4} A_{nn}^{<, \text{real}} B_{nn}^{<, \text{real}} + \frac{1}{4} A_{nn}^{>, \text{real}} B_{nn}^{<, \text{real}} + \frac{1}{4} A_{nn}^{<, \text{real}} B_{nn}^{>, \text{real}} + \frac{1}{4} A_{nn}^{>, \text{real}} B_{nn}^{>, \text{real}} \right\} \Delta t, \quad (36)$$

where we have used explicitly Eq. (19). Therefore, it is necessary to add a correction

$$(\delta(A * B))_{nn} = (C_1)_{nn} - (\tilde{C}_1)_{nn} \equiv (\Delta C_1)_{nn} \quad (37)$$

to Eq. (36) in order to recover Eq. (35):

$$(\delta(A * B))_{nn} = \left(\frac{1}{4} A_{nn}^{>, \text{real}} B_{nn}^{<, \text{real}} + \frac{1}{4} A_{nn}^{<, \text{real}} B_{nn}^{>, \text{real}} - \frac{1}{4} A_{nn}^{<, \text{real}} B_{nn}^{<, \text{real}} - \frac{1}{4} A_{nn}^{>, \text{real}} B_{nn}^{>, \text{real}} \right) \Delta t = -\Delta A_{nn} \Delta B_{nn} \Delta t. \quad (38)$$

Importantly, if we didn't include the corrections (38), using Eq. (36) instead of Eq. (35) in our numerical implementation, this would imply an error $\propto \Delta t$.

Corrections similar to Eq. (38) are necessary not only in the diagonal elements of $C(t, t)$, but also every time at least one of t, t' is 0, t_{\max}, β , i.e. boundary terms in t and/or t' . For example, in computing $C(0, t)$ the exact integral contains $A_{00}^{<, \text{real}} \bar{B}_{0n}$, while we compute $\bar{A}_{00} \bar{B}_{0n}$. Combining all the boundary terms, a total of 72 different corrections are needed, plus the already discussed corrections for the diagonal terms.

Inversion and solution of the Dyson equation

The Dyson equations (9) can be easily recast in the integral form

$$(1 + F) * Y = C, \quad (39)$$

where $F = -G_0 * \Sigma$, $C = G_0$ and $Y = G$ is the unknown function. The DMFT equations for both the FKM and the Hubbard model, described later in the text, can be expressed in the form of Eq. (39).

Equations in the regularized form of Eq. (39) can be numerically solved in a straightforward manner using our matrix representation of the Green's functions (see Eqs. (19) and (20)). To this aim, we need first to compute the jump of Y , and second, find the corrections to Y due to the correction $\delta(F * Y)$ (see Eq. (37)) coming from the convolution. For the first point, we note

that the diagonal elements of $\bar{Y}(t_n, t_n)$ and $\Delta Y(t_n)$ are *independent* variables which in principle satisfy different equations. We now observe that C has a jump, while $(1 + F)$ has not because it contains the result of a convolution. Equation (39) then implies

$$\Delta Y(t_n) = \Delta C(t_n) \quad (40)$$

for the vector of the differences.

If we knew Y , we would be able to compute the convolution $F * Y$ with all the corrections. On the other side, if none of the functions F , Y or C had a jump, Eq. 39 would be a simple linear system:

$$(1 + \bar{F}\bar{w})\bar{Y}_0 = \bar{C}, \quad (41)$$

where \bar{w} is the vector of the integration weights. We now show that we can find \bar{Y} solving equations of the form (41) and using Newton iteration. Indeed we can view the left-hand side of Eq. (39) as a functional \mathcal{F} of Y and write

$$\mathcal{F}(Y) = C, \quad (42)$$

with

$$\mathcal{F}(Y) = (1 + \bar{F}\bar{w})\bar{Y} + \delta(F * Y), \quad (43)$$

where $\bar{F}\bar{w}\bar{Y}$ is the contribution to the convolution coming only from the matrix \bar{Y} and $\delta(F * Y)$ contains the corrections. As a starting guess for \bar{Y} we take \bar{Y}_0 , i.e. the solution of Eq. (41). Notice that we already know the exact solution for ΔY (see Eq. (40)), but for convenience we also define $\Delta Y_0 \equiv \Delta Y$. Knowing \bar{Y}_0 and ΔY_0 we can now compute $\mathcal{F}[Y_0]$, which contains the full convolution $F * Y_0$, i.e. also the contribution of ΔY_0 . Next, we need the derivative of F in \bar{Y}_0 , which can be approximated as

$$\left. \frac{d\mathcal{F}}{d\bar{Y}} \right|_{\bar{Y}=\bar{Y}_0} \approx (1 + \bar{F}\bar{w}). \quad (44)$$

If we define \bar{Y}_1 as the first correction to Y_0 , the difference $\delta\bar{Y}_1 \equiv \bar{Y}_1 - \bar{Y}_0$ satisfies

$$\delta\bar{Y}_1 = (1 + \bar{F}\bar{w})^{-1} (\bar{C} - \bar{Y}_0 - \bar{F}\bar{w}\bar{Y}_0 - \delta(F * Y_0)). \quad (45)$$

At the $(n + 1)$ -th iteration we similarly find

$$\delta\bar{Y}_{n+1} = (1 + \bar{F}\bar{w})^{-1} (\bar{C} - \bar{Y}_n - \bar{F}\bar{w}\bar{Y}_n - \delta(F * Y_n)). \quad (46)$$

In practice the iteration quickly converges to $\delta Y_n = 0$, which implies that Y satisfies Eq. (42).

DMFT solutions

DMFT requires the solution of the local Green's function $G_{ii} \equiv G$ from an impurity model with action:

$$\mathcal{S} = -i \int_C dt' H_{\text{loc}}(t') - i \int_C dt_1 dt_2 \Lambda(t_1, t_2) c_\sigma^\dagger(t_1) c_\sigma(t_2), \quad (47)$$

where H_{loc} is the local part of the Hamiltonian, and the hybridization function $\Lambda(t_1, t_2)$ is determined self-consistently. As stated in the main text, we consider a Bethe lattice in the infinite coordination limit $Z \rightarrow \infty$, with the V_{ij} corresponding to a semi-elliptic density of states:

$$\rho(\epsilon) = \frac{1}{L} \sum_k \delta(\epsilon - \epsilon_k) = \frac{1}{2\pi V} \sqrt{4V^2 - \epsilon^2}, \quad (48)$$

which allows a closed form of the self-consistency: $\Lambda(t_1, t_2) = V^2 G(t_1, t_2)$ [33].

As in the standard nonequilibrium case, the solution of the nonequilibrium problem, i.e., the evaluation of the Green's function from the expectation value $G(t_1, t_2) = -i \text{Tr}[\mathcal{T}_C e^{-\mathcal{S}} c(t_1) c^\dagger(t_2)] / \text{Tr}[\mathcal{T}_C e^{-\mathcal{S}}]$, is numerically the most challenging part. However, all approaches based on perturbation expansions can be readily rewritten, including numerically exact Quantum Monte Carlo algorithms [35] (used in the context of the Hubbard model), and closed equations of motion (used in the context of the Falicov-Kimball model) [38].

Below we illustrate the DMFT solution of the Falicov-Kimball and the Hubbard model. In both cases the lattice Hamiltonian has the contour-dependent form:

$$H(t) = \begin{cases} H & \text{if } t \in \mathcal{C}_1 \\ H_0 & \text{if } t \in \mathcal{C}_2 \\ H_0 & \text{if } t \in \mathcal{C}_3, \end{cases} \quad (49)$$

where

$$H = H_0 + U \sum_i n_{i\uparrow} n_{i\downarrow}. \quad (50)$$

Exact DMFT solution of the FKM

The DMFT equations for the Falicov-Kimball model are formally identical to the sudden-quench case [40, 51], the only difference being in the explicit contour-dependence of the Hamiltonian. However, this difference plays an important role, since in the standard case the problem has also an analytical solution [40], while in our case we have to resort to a numerical solution.

The central quantity for the DMFT solution is the local Green's function $G(t, t')$ of the itinerant fermions, which is a weighted sum of two components [40]:

$$G(t, t') = w_0 Q(t, t') + w_1 R(t, t'). \quad (51)$$

In particular, the component $Q(t, t')$ describes lattice sites where immobile electrons are absent, while the component $R(t, t')$ takes into account the presence of the potential due to the f -electrons. The weight $w_1 = 1 - w_0$ is the average number of localized particles and we take $w_0 = 0.5$, i.e. half-filling. The expectation value of the

double occupancy $d_{\text{FK}}(t)$ is easily computed within the DMFT formalism from the Green's function:

$$d_{\text{FK}}(t) = -iw_1 R^{<,1}(t, t), \quad (52)$$

where the lesser component of R is defined as

$$R^{<,1}(t, t) \equiv \lim_{t' \rightarrow t^+} R_{11}(t, t'), \quad (53)$$

keeping in mind the matrix structure (16).

We briefly recall now the steps of the DMFT self-consistency loop. Starting from some initial guess for the hybridization $\Delta(t, t')$, the local Green's function (51) can be determined solving [40]

$$[i\partial_t + \mu] Q(t, t') - \Delta * Q(t, t') = \delta_{\mathcal{C}}(t, t'), \quad (54)$$

$$[i\partial_t + \mu - U(t)] R(t, t') - \Delta * R(t, t') = \delta_{\mathcal{C}}(t, t'), \quad (55)$$

where $(i\partial_t + \mu) \equiv g_0^{-1}$ is the inverse of the single-particle, noninteracting Green's function (we similarly define also $(i\partial_t + \mu - U(t)) \equiv g_1^{-1}$). In Eqs. (54) and (55) $\delta_{\mathcal{C}}(t, t')$ is the contour delta function satisfying

$$\delta_{\mathcal{C}}(t, t') = \partial_t \theta_{\mathcal{C}}, \quad \int_{\mathcal{C}} d\bar{t} \delta_{\mathcal{C}}(t, \bar{t}) g(\bar{t}) = g(t) \quad \forall g(t), \quad (56)$$

with the time derivative defined according to the branch:

$$\partial_t g(t) = \begin{cases} \partial_t g(t^{\pm}) & t \in \mathcal{C}_{1,2} \\ i\partial_{\tau} g(-i\tau) & t = -i\tau \in \mathcal{C}_3. \end{cases} \quad (57)$$

The numerical implementation of the derivative and the delta function is nontrivial, as discussed in Ref. 39. However we avoid this problem because we do not solve directly Eqs. (54) and (55), but rather their integral version:

$$(1 - g_0 * \Delta) * Q = g_0, \quad (58)$$

$$(1 - g_1 * \Delta) * R = g_1. \quad (59)$$

The next step is computing the new hybridization function from the knowledge of $G(t, t')$. This becomes a simple task if the semi-elliptic density of states is assumed [40] (as we do in the main text):

$$\Delta(t, t') = V^2 G(t, t'). \quad (60)$$

where V is the hopping energy scale. With this new solution for the hybridization, a new iteration starts by inserting Δ in Eqs. (58) and (59). The set of equations (51), (58), (59) and (60) is solved self-consistently until convergence is reached. For the results shown in this paper, the convergence criterion is defined by

$$\varepsilon = \max_{i \in [0, N]} |\Re(d_{\text{FK}}(t_i)^{(n+1)}) - \Re(d_{\text{FK}}(t_i)^{(n)})|, \quad (61)$$

which compares the real part of the double occupancies at the (n) -th and the previous DMFT iteration, terminating the computation if $\varepsilon < \varepsilon_{\text{max}}$. Typical values of ε_{max} are $\sim 10^{-6}$.

With the self-consistency equations displayed above, the number of iterations n_{iter} necessary for the DMFT to converge is naively expected to increase both with the interaction U and with the maximum time t_{max} up to which the evolution is calculated. However, in the presence of coexisting solutions, also at short or intermediate times n_{iter} can become large. A way to accelerate convergence is slightly modifying the self-consistency step, so that the hybridization function at iteration $(n+1)$ is constructed from a combination of the newly-computed Green's function $G^{(n)}(t, t')$ and the $G^{(n-1)}(t, t')$ obtained at the previous step:

$$\Delta^{(n+1)}(t, t') = V^2 \left(G^{(n-1)}(t, t') + \gamma (G^{(n)}(t, t') - G^{(n-1)}(t, t')) \right). \quad (62)$$

The parameter γ controls the mixing of the two solutions, $\gamma = 1$ corresponding to the case of Eq. (60).

DMFT solution of the Hubbard model with continuous-time Monte Carlo

A numerically exact solution of the nonequilibrium DMFT equations for the Hubbard model can be obtained with a continuous-time Monte Carlo impurity solver. The weak-coupling approach [35, 43] uses the noninteracting impurity Green's function G_0 as an input. This function is related to the hybridization function Δ by

$$G_0^{-1}(t, t') = (i\partial_t + \mu)\delta_{\mathcal{C}}(t, t') - \Delta(t, t'). \quad (63)$$

The quantity measured in the Monte Carlo simulation is the improper self-energy [30, 35] $X(t_1, t_2)$, which is related to the noninteracting impurity Green's function G_0 and self-energy Σ by

$$X_{\sigma} * G_{0,\sigma} = \Sigma_{\sigma} * G_{0,\sigma}. \quad (64)$$

Using the Dyson equation (9) and Eq. (64) we obtain the relation

$$(1 + X_{\sigma} * G_{0,\sigma}) * \Sigma_{\sigma} = X_{\sigma}, \quad (65)$$

which for given X_{σ} can be solved in a stable manner to yield the self-energy. Once the self-energy is obtained, the DMFT self-consistency step is performed as follows: the new hybridization function Δ is found via the Dyson equation (9) and the self-consistency equation (60), and then the new noninteracting Green's function G_0 results from inverting Eq. (63). The double occupancy is extracted from the relation

$$U(t) \langle n_{\sigma}(t) [n_{\sigma}(t) - \frac{1}{2}] \rangle = -i [\Sigma * G_{\sigma}]^{<}(t, t). \quad (66)$$

[1] T. Kinoshita, T. Wenger, and D. S. Weiss, *Nature* **440**, 900 (2006).

- [2] I. Bloch, J. Dalibard, and W. Zwerger, *Rev. Mod. Phys.* **80**, 885 (2008).
- [3] R. Jördens, N. Strohmaier, K. Günter, H. Moritz, and T. Esslinger, *Nature* **455**, 204 (2008).
- [4] U. Schneider, L. Hackermüller, S. Will, T. Best, I. Bloch, T. A. Costi, R. W. Helmes, D. Rasch, and A. Rosch, *Science* **322**, 1520 (2008).
- [5] S. Iwai, M. Ono, A. Maeda, H. Matsuzaki, H. Kishida, H. Okamoto, and Y. Tokura, *Phys. Rev. Lett.* **91**, 057401 (2003).
- [6] L. Perfetti, P. A. Loukakos, M. Lisowski, U. Bovensiepen, H. Berger, S. Biermann, P. S. Cornaglia, A. Georges, and M. Wolf, *Phys. Rev. Lett.* **97**, 067402 (2006).
- [7] S. Wall, D. Brida, S. R. Clark, H. P. Ehrke, D. Jaksch, A. Ardavan, S. Bonora, H. Uemura, Y. Takahashi, T. Hasegawa, H. Okamoto, G. Cerullo, and A. Cavalleri, *Nature Phys.* **7**, 114 (2011).
- [8] A. Polkovnikov, K. Sengupta, A. Silva, and M. Vengalattore, *Rev. Mod. Phys.* **83**, 863 (2011).
- [9] M. Rigol, V. Dunjko, V. Yurovsky, and M. Olshanii, *Phys. Rev. Lett.* **98**, 050405 (2007).
- [10] J. Berges, S. Borsányi, and C. Wetterich, *Phys. Rev. Lett.* **93**, 142002 (2004).
- [11] M. Moeckel and S. Kehrein, *Phys. Rev. Lett.* **100**, 175702 (2008).
- [12] M. Kollar, F. A. Wolf, and M. Eckstein, *Phys. Rev. B* **84**, 054304 (2011).
- [13] M. Eckstein, M. Kollar, and P. Werner, *Phys. Rev. Lett.* **103**, 056403 (2009).
- [14] M. Schirò and M. Fabrizio, *Phys. Rev. B* **83**, 165105 (2011).
- [15] J. Berges, A. Rothkopf, and J. Schmidt, *Phys. Rev. Lett.* **101**, 041603 (2008).
- [16] B. Sciolia and G. Biroli, *Phys. Rev. Lett.* **105**, 220401 (2010).
- [17] N. Tsuji, M. Eckstein, and P. Werner, *Phys. Rev. Lett.* **110**, 136404 (2013).
- [18] M. Heyl, A. Polkovnikov, and S. Kehrein, *Phys. Rev. Lett.* **110**, 135704 (2013).
- [19] The expression “dynamical phase transition” also appears in the literature with another meaning, e.g. in Ref. [13] it refers to a transition between different relaxation regimes. In this paper we strictly adhere to the definition given by Heyl et al. [18].
- [20] Note that differently from the partition function in equilibrium an overlap $A(t)$ can become zero also for finite systems, which would imply a non-analytic behavior of $a(it)$. Such orthogonalities [22, 26, 52–54] usually rely on certain resonances between many-body eigenstates. For a generic finite quantum system $A(t)$ is nonzero for all times, making DPTs a unique phenomenon appearing in the thermodynamic limit.
- [21] M. Fagotti, ArXiv e-prints (2013), arXiv:1308.0277 [cond-mat.stat-mech].
- [22] F. Andraschko and J. Sirker, *Phys. Rev. B* **89**, 125120 (2014).
- [23] M. Heyl, ArXiv e-prints (2014), arXiv:1403.4570 [cond-mat.stat-mech].
- [24] M. Heyl and M. Vojta, ArXiv e-prints (2013), arXiv:1310.6226 [cond-mat.dis-nn].
- [25] Z.-X. Gong and L.-M. Duan, *New Journal of Physics* **15**, 113051 (2013).
- [26] C. Karrasch and D. Schuricht, *Phys. Rev. B* **87**, 195104 (2013).
- [27] S. Vajna and B. Dóra, *Phys. Rev. B* **89**, 161105 (2014).
- [28] J. M. Hickey, S. Genway, and J. P. Garrahan, *Phys. Rev. B* **89**, 054301 (2014).
- [29] J. Kriel, C. Karrasch, and S. Kehrein, arXiv e-prints (2014), arXiv:1407.4036 [cond-mat.stat-mech].
- [30] H. Aoki, N. Tsuji, M. Eckstein, M. Kollar, T. Oka, and P. Werner, *Rev. Mod. Phys.* **86**, 779 (2014).
- [31] J. W. Negele and H. Orland, *Quantum Many-Particle Systems* (Addison-Wesley, Redwood City, 1988).
- [32] For example, when Y is the double occupancy in the Hubbard model as below, this means a short switch-off of the hopping.
- [33] A. Georges, G. Kotliar, W. Krauth, and M. J. Rozenberg, *Rev. Mod. Phys.* **68**, 13 (1996).
- [34] W. Metzner and D. Vollhardt, *Phys. Rev. Lett.* **62**, 324 (1989).
- [35] P. Werner, T. Oka, M. Eckstein, and A. J. Millis, *Phys. Rev. B* **81**, 035108 (2010).
- [36] U. Brandt and C. Mielsch, *Z. Phys. B: Condens. Matter* **75**, 365 (1989).
- [37] J. K. Freericks and V. Zlatić, *Rev. Mod. Phys.* **75**, 1333 (2003).
- [38] J. K. Freericks, V. M. Turkowski, and V. Zlatić, *Phys. Rev. Lett.* **97**, 266408 (2006).
- [39] J. K. Freericks, *Phys. Rev. B* **77**, 075109 (2008).
- [40] M. Eckstein and M. Kollar, *Phys. Rev. Lett.* **100**, 120404 (2008).
- [41] M. Eckstein and M. Kollar, *New J. Phys.* **12**, 055012 (2010).
- [42] B. Moritz, A. F. Kemper, M. Sentef, T. P. Devereaux, and J. K. Freericks, *Phys. Rev. Lett.* **111**, 077401 (2013).
- [43] P. Werner, T. Oka, and A. J. Millis, *Phys. Rev. B* **79**, 035320 (2009).
- [44] S. Vajna and B. Dóra, ArXiv e-prints (2014), arXiv:1409.7019 [cond-mat.str-el].
- [45] F. Albuquerque, A.F. Alet, P. Corboz, P. Dayal, A. Feiguin, S. Fuchs, L. Gamper, E. Gull, S. Gürtler, A. Honecker, R. Igarashi, M. Körner, A. Kozhevnikov, A. Läuchli, S. Manmana, M. Matsumoto, I. McCulloch, F. Michel, R. Noack, G. Pawłowski, L. Pollet, T. Pruschke, U. Schollwöck, S. Todo, S. Trebst, M. Troyer, P. Werner, and S. Wessel, *Journal of Magnetism and Magnetic Materials* **310**, 1187 (2007).
- [46] H. S. Köhler, N. H. Kwong, and H. A. Yousif, *Comput. Phys. Comm.* **123**, 123 (1999).
- [47] M.-T. Tran, *Phys. Rev. B* **78**, 125103 (2008).
- [48] A. Stan, N. E. Dahlen, and R. van Leeuwen, *J. Chem. Phys.* **130**, 224101 (2009).
- [49] M. Eckstein, M. Kollar, and P. Werner, *Phys. Rev. B* **81**, 115131 (2010).
- [50] K. Balzer and M. Bonitz, *Nonequilibrium Green's Functions Approach to Inhomogeneous Systems*, Lecture Notes in Physics, Vol. 867 (Springer, Heidelberg, Germany, 2013).
- [51] M. Eckstein and M. Kollar, *Phys. Rev. B* **78**, 245113 (2008).
- [52] M. Ligare and R. Oliveri, *American Journal of Physics* **70**, 58 (2002).
- [53] H. Gießen, J. D. Berger, G. Mohs, P. Meystre, and S. F. Yelin, *Phys. Rev. A* **53**, 2816 (1996).
- [54] G. Stey and R. Gibberd, *Physica* **60**, 1 (1972).